Sensors and Materials, Vol. 34, No. 2 (2022) 707–715
MYU Tokyo

S & M 2845

Radiation Response Characteristics of Pr^{3+}-activated $SrO–Al_2O_3–TeO_2$ Glasses

Ryogo Nakamori,[1*] Naoki Kawano,[1] Akito Takaku,[1]
Daichi Onoda,[2] Yuma Takebuchi,[2] Hiroyuki Fukushima,[2]
Takumi Kato,[2] Kenji Shinozaki,[3] and Takayuki Yanagida[2]

[1]Graduate School of Engineering Science, Akita University,
1-1 Tegata-Gakuen-machi, Akita 010-8502, Japan
[2]Graduate School of Materials Science, Nara Institute of Science and Technology (NAIST),
8916-5 Takayama, Ikoma 630-0192, Japan
[3]National Institute of Advanced Industrial Science and Technology (AIST),
1-8-31 Midorigaoka, Ikeda-shi, Osaka 563-8577, Japan

(Received October 13, 2021; accepted November 17, 2021)

Keywords: scintillator, Pr, luminescence, glass, tellurite

We fabricated Pr^{3+}-activated glasses having a composition of $10SrO–5Al_2O_3–85TeO_2$ (PSAT) for potential use as radiation detectors, and their photoluminescence (PL) and X-ray-induced scintillation properties were then characterized. The PSAT glasses showed several emission peaks in their PL spectra owing to the 4f–4f transitions of Pr^{3+}. Furthermore, they exhibited typical PL decay times (0.09–0.86 ms), where the decay originated from the 4f–4f transitions of Pr^{3+}. In the scintillation spectra of the PSAT glasses, three peaks at approximately 480, 618, and 636 nm were observed. The scintillation decay times were 0.747–0.840 ms, corresponding to the 4f–4f transitions of Pr^{3+}. Furthermore, the PSAT glasses showed afterglow levels of 352–521 ppm, and the lowest afterglow level (352 ppm) was comparable to that of Tl-activated CsI single crystal.

1. Introduction

Scintillators have been used as luminescence materials for radiation detection, and they have the function of changing high-energy ionizing radiation into a large number of low-energy photons.(1) They have been used in a wide variety of fields such as high-energy physics and nuclear medicine.(2,3) Single-crystal scintillators have often been used in these fields because they tend to show high light yields. Glass scintillators have recently attracted research attention because of their industrial merits such as low cost, excellent moldability, flexible glass composition, and the possibility of large-volume production.(4–10) The scintillation properties of many glasses doped with a rare-earth (RE) ion, such as Dy^{3+}-activated $B_2O_3–Al_2O_3–SrO$ glasses and Eu^{3+}-activated $K_2O–Bi_2O_3–Ga_2O_3$ glasses, have been evaluated.(11,12)

Tellurite glasses are also potential glass scintillators. Tellurite glasses can exhibit high detection efficiency under X- and γ-ray exposure because of their high effective atomic number.

*Corresponding author: e-mail: m8021210@s.akita-u.ac.jp
https://doi.org/10.18494/SAM3689

ISSN 0914-4935

In addition, it might be possible to suppress their non-radiative decay since their phonon energy is lower than that of other glasses (e.g., phosphate glasses, borate glasses, and silicate glasses); therefore, they might exhibit higher PL and scintillation intensity.[13–18] So far, several tellurite glasses such as Nd^{3+}-activated $15WO_3–5Al_2O_3–80TeO_2$ glasses, Eu^{3+}-activated $15BaO–5Al_2O_3–80TeO_2$ glasses, Dy^{3+}-activated $15BaO–5Al_2O_3–80TeO_2$ glasses, and Eu^{3+}-activated $10SrO–5Al_2O_3–85TeO_2$ glasses have been studied as possible radiation detectors.[15–18] In this paper, we focus on Pr^{3+}-activated tellurite glasses. Pr^{3+} ions have been widely used as luminescence centers because Pr^{3+}-activated materials such as Pr^{3+}-activated Gd_2O_2S can exhibit efficient luminescence originating from the 4f–4f transitions of Pr^{3+}.[19–21] In this work, glasses having compositions of $xPr_2O_3–(10−x)SrO–5Al_2O_3–85TeO_2$ (x = 0.1, 0.5, and 1.0) (PSAT) (Z_{eff} = 44.5–44.7) were fabricated by the melt-quenching technique and we investigated their PL and scintillation properties.

2. Experimental Methods

The PSAT glasses listed in Table 1 were prepared as follows. As precursors, Pr_2O_3, $SrCO_3$, Al_2O_3, and TeO_2 were obtained from Kojundo Chemical Lab. Co., Ltd. They were mixed in the above glass composition, and the mixture was heated in an aluminum crucible in air for 1 h inside an electric furnace whose temperature was 950 °C. The heated mixture was poured on a plate that had been preheated at approximately 300 °C to fabricate the PSAT glasses. PSAT glasses with a thickness of approximately 1.5 mm and a mass of approximately 0.41 g, which were used for characterization, were obtained by polishing the glasses.

The glass transition temperature (T_g) was measured by using an analyzer (TG-DTA2000SA, Bruker). The crystalline phase in the PSAT glasses was investigated using an X-ray diffractometer (RINT-2200 V, RIGAKU). As optical characteristics, optical in-line transmittance spectra were measured using a spectrometer (V670, JASCO) with the aim of investigating the absorption properties of the PSAT glasses. In addition, PL quantum yield (QY) values and PL excitation and emission maps were recorded using a spectrometer (Quantaurus-QY, Hamamatsu). Moreover, PL spectra and PL excitation spectra were recorded using a spectrometer (RF-6000, Shimadzu). PL decay curves were also measured using a PL spectrometer (Quantaurus-τ, Hamamatsu) with the aim of determining the PL decay times. As scintillation characteristics, scintillation spectra were recorded using our original setup, details of which are given in Ref. 22. The voltage and current of the X-ray tube in the setup used to generate X-rays were set to 80 kV and 1.2 mA, respectively. Furthermore, our original evaluation

Table 1
Compositions of PSAT glasses.

Sample code	Glass composition
0.1PSAT	$0.1Pr_2O_3–9.9SrO–5Al_2O_3–85TeO_2$
0.5PSAT	$0.5Pr_2O_3–9.5SrO–5Al_2O_3–85TeO_2$
1.0PSAT	$1Pr_2O_3–9SrO–5Al_2O_3–85TeO_2$

system, details of which are given in Ref. 23, was used for the measurement of pulse-X-ray-induced decay curves and afterglow curves.

3. Results and Discussion

3.1 Samples

A photograph of the PSAT glasses is shown in Fig. 1. All the PSAT glasses were transparent. In addition, the 0.1PSAT glass was yellow, whereas the 0.5PSAT and 1.0PSAT glasses were green.

Table 2 summarizes the T_g values of the PSAT glasses. T_g values were obtained in all of the PSAT glasses, indicating the formation of the glasses.[24] The T_g values were almost the same for the fabricated PSAT glasses.

X-ray diffraction (XRD) patterns of the PSAT glasses are shown in Fig. 2. All the PSAT glasses showed a halo peak, and no sharp peaks derived from a crystalline phase were observed; therefore, all the PSAT glasses were found to be amorphous.[4,18]

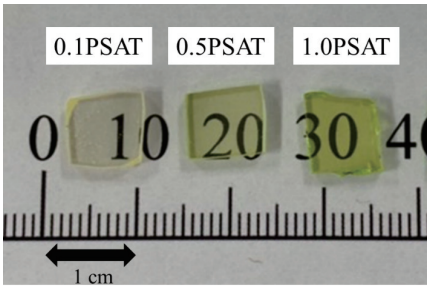

Fig. 1. (Color online) Photograph of the PSAT glasses.

Table 2
T_g values of the PSAT glasses.

	0.1PSAT	0.5PSAT	1.0PSAT
T_g (°C)	399.4	402.5	403.0

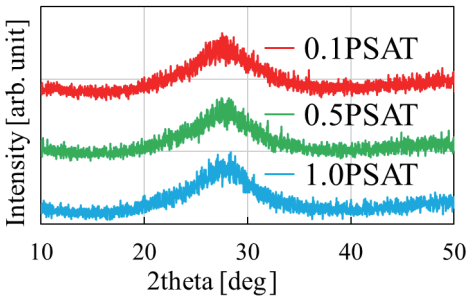

Fig. 2. (Color online) XRD patterns of the PSAT glasses.

3.2 Absorption and photoluminescence properties

Figure 3 shows in-line transmittance spectra of the PSAT glasses across the wavelength range of 200–2700 nm. The transmittances of the PSAT glasses were approximately 70–80%. Furthermore, in all the PSAT glasses, some absorption bands originating from the 4f–4f transitions of Pr^{3+} appeared at approximately 449 nm ($^3H_4 \rightarrow {}^3P_2$), 473 nm ($^3H_4 \rightarrow {}^3P_1$), 486 nm ($^3H_4 \rightarrow {}^3P_0$), 595 nm ($^3H_4 \rightarrow {}^1D_2$), 1023 nm ($^3H_4 \rightarrow {}^1G_4$), 1439 nm ($^3H_4 \rightarrow {}^3F_4$), 1540 nm ($^3H_4 \rightarrow {}^3F_3$), and 1952 nm ($^3H_4 \rightarrow {}^3F_2$).[19,25] The absorption intensity of the PSAT glasses increased with the amount of Pr_2O_3 doping. Moreover, the absorption edges were almost the same in the PSAT glasses.

Figure 4 presents the PL excitation and emission map of the 0.1PSAT glass. Several emission peaks were detected under excitation wavelengths of 440–490 nm. Figure 5 shows PL spectra of the PSAT glasses under an excitation wavelength of 450 nm. Some emission peaks originating from the 4f–4f transitions of Pr^{3+} appeared at 488 nm ($^3P_{0,1} \rightarrow {}^3H_4$), 532 nm ($^3P_1 \rightarrow {}^3H_5$), 545 nm ($^3P_0 \rightarrow {}^3H_5$), 614 nm ($^3P_0 \rightarrow {}^3H_6$), and 646 nm ($^3P_0 \rightarrow {}^3F_2$) in all the PSAT glasses. In addition, PL excitation spectra of the PSAT glasses under an emission wavelength of 646 nm are shown in Fig. 6. All the PSAT glasses showed excitation peaks at 445, 473, and 484 nm due to the 4f–4f

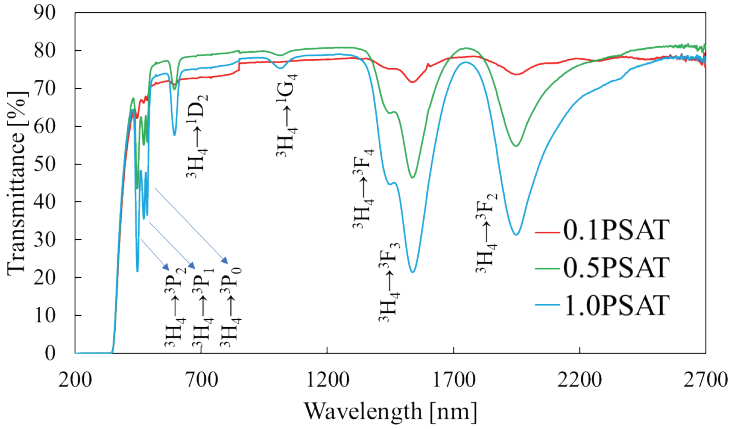

Fig. 3. (Color online) In-line transmittance spectra of the PSAT glasses.

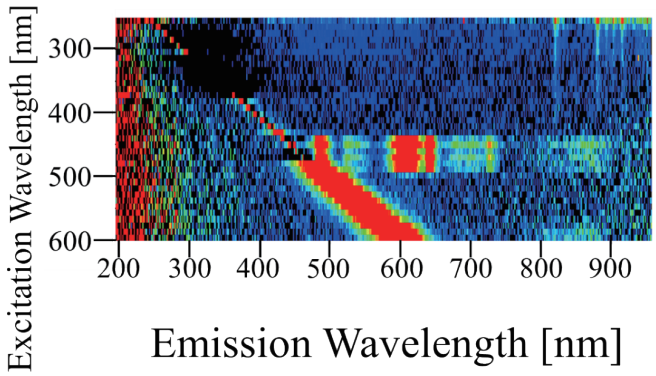

Fig. 4. (Color online) PL excitation and emission map of the 0.1PSAT glass.

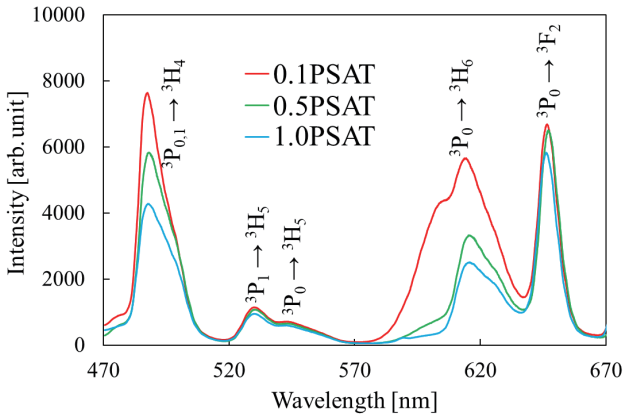

Fig. 5. (Color online) PL spectra of the PSAT glasses under an excitation wavelength of 450 nm.

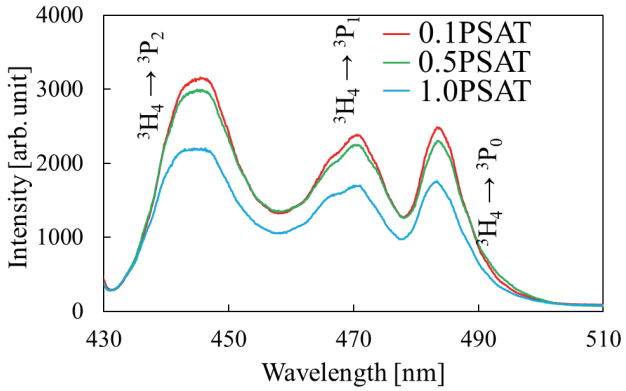

Fig. 6. (Color online) PL excitation spectra of the PSAT glasses under an emission wavelength of 646 nm.

transitions ($^3H_4 \rightarrow {}^3P_2$, $^3H_4 \rightarrow {}^3P_1$, and $^3H_4 \rightarrow {}^3P_0$, respectively) of Pr^{3+}.[26–30] Moreover, the *QY* values of the PSAT glasses were 26% (0.1PSAT), 17% (0.5PSAT), and 8% (1.0PSAT), as listed in Table 3, and the *QY* values decreased with increasing Pr_2O_3 concentration, probably because of concentration quenching.

PL decay curves of the PSAT glasses under an excitation wavelength of 450 nm are shown in Fig. 7. The monitoring wavelength was 610 nm. The PL decay times of the PSAT glasses were calculated by approximating the curves with an exponential decay function. The decay times were 0.86 ms (0.1PSAT), 0.15 ms (0.5PSAT), and 0.09 ms (1.0PSAT). The decay time of the 0.1PSAT glass was typical for the 4f–4f transition ($^3P_0 \rightarrow {}^3H_6$) of Pr^{3+}.[31] Moreover, the decrease in the decay time with increasing Pr_2O_3 concentration might be due to concentration quenching, and strong concentration quenching should occur in 1.0PSAT in particular because its decay time was much shorter than the typical decay time for the 4f–4f transitions of Pr^{3+}.[17]

3.3 Scintillation properties

X-ray-induced scintillation spectra of the PSAT glasses are shown in Fig. 8. All the PSAT glasses showed three scintillation peaks at approximately 480 nm ($^3P_{0,1} \rightarrow {}^3H_4$), 618 nm

Table 3
QY values of the PSAT glasses under an excitation wavelength of 450 nm.

Sample code	0.1PSAT	0.5PSAT	1.0PSAT
QY value (%)	26	17	8

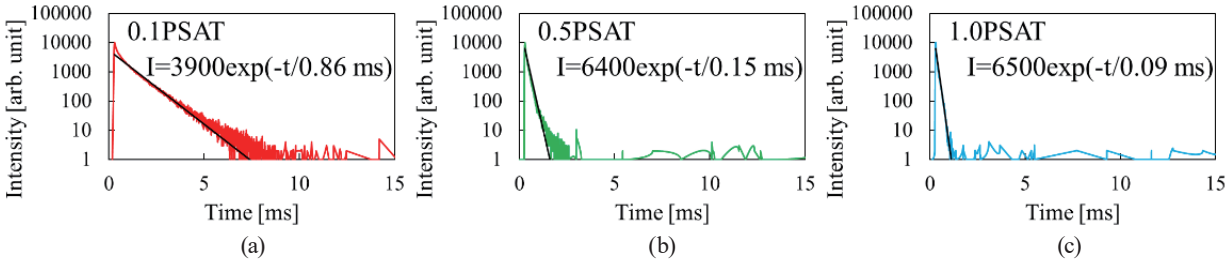

Fig. 7. (Color online) PL decay curves of (a) 0.1PSAT glass, (b) 0.5PSAT glass, and (c) 1.0PSAT glass.

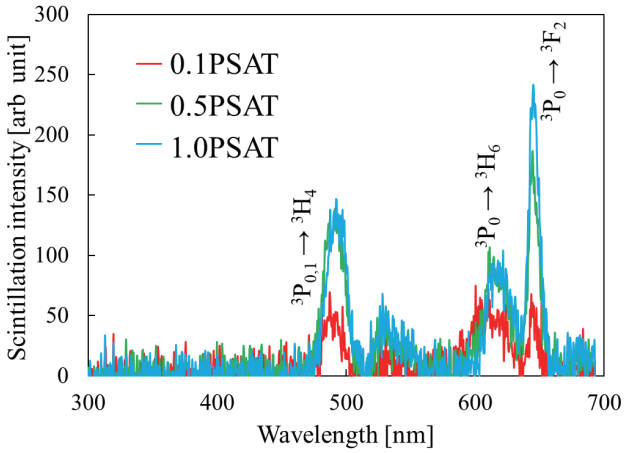

Fig. 8. (Color online) X-ray-induced scintillation spectra of the PSAT glasses.

($^3P_0 \rightarrow {}^3H_6$), and 636 nm ($^3P_0 \rightarrow {}^3F_2$). These peaks originated from the 4f–4f transitions of Pr^{3+}.[21] Contrary to the results obtained from the PL spectra in Fig. 5, the integrated scintillation intensity across the range of 470–670 nm increased with increasing Pr_2O_3 concentration. On the basis of theoretical works, the scintillation intensity can be calculated as[32,33]

$$LY \propto \frac{E_r}{\beta E_g} \times S \times QY. \tag{1}$$

Here, LY is the scintillation intensity, E_g is the band gap energy of the material, E_r is the energy of the ionizing radiation, S is the energy transfer efficiency, β is a constant, and QY is the quantum yield. In this work, the integrated scintillation intensity of the PSAT glasses was found to be inversely proportional to the QY value as shown in Fig. 9. The almost equal band gap energies of the fabricated PSAT glasses might have been because the absorption edges of the

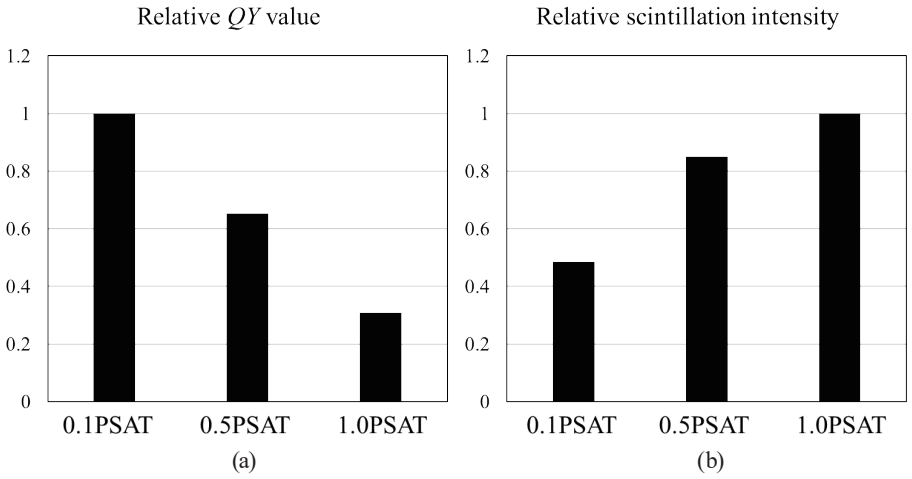

Fig. 9. (a) Relative *QY* value and (b) relative scintillation intensity.

PSAT glasses were almost equal; therefore, it is suggested that the energy transfer efficiency was increased by the Pr_2O_3 doping. It is known that the efficiency is affected by the number of trapping sites. In the case of glass materials, non-bridging oxygen should be one of the candidate trapping centers according to past studies,[34,35] and the amount of non-bridging oxygen is reported to increase with increasing amount of glass modifiers such as SrO.[35,36] The number of trapping sites (e.g., non-bridging oxygen) might be decreased by the replacement of SrO with Pr_2O_3,[18,34–36] leading to enhanced energy transfer efficiency.

Figure 10 presents X-ray-induced scintillation decay curves of the PSAT glasses. The decay times were calculated as the sum of two exponential functions. The first decay times (0.016–0.017 ms) should originate from the instrumental response. In addition, the second decay times of the 0.1PSAT, 0.5PSAT, and 1.0PSAT glasses were 0.840, 0.795, and 0.747 ms, respectively. The second decay times should originate from the 4f–4f transitions of Pr^{3+}.[21] Moreover, the second decay times of the PSAT glasses decreased with increasing Pr_2O_3 concentration. This should be due to concentration quenching because the decay times decreased with increasing Pr_2O_3 concentration.[37]

Afterglow profiles of the PSAT glasses are shown in Fig. 11. Afterglow levels were calculated using[30,38]

$$I[\%] = 100 \times \frac{I_x - I_B}{I_{20} - I_B}, \tag{2}$$

where I_x is the average intensity when the tellurite glasses were excited by X-rays, I_{20} is the intensity 20 ms after the end of X-ray exposure, and I_B is the intensity of the background. The afterglow levels of the 0.1PSAT, 0.5PSAT, and 1.0PSAT glasses were 521, 459, and 352 ppm, respectively. The 1.0PSAT glass showed a low afterglow level (352 ppm) comparable to that of Tl-activated CsI single crystal.[23] It is known that afterglow is a luminescence phenomenon associated with complex trapping and detrapping processes of carriers at room temperature. The

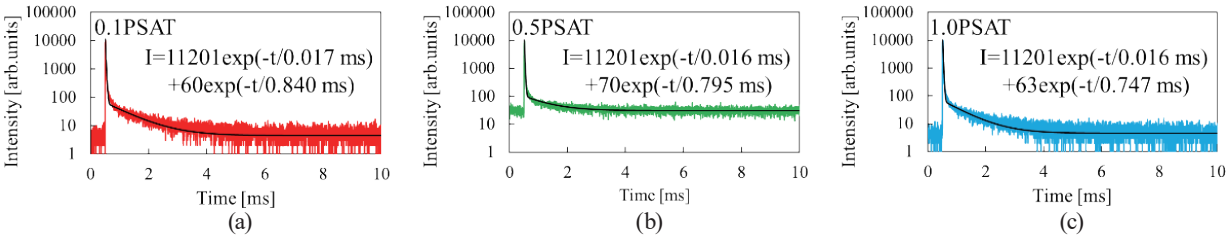

Fig. 10. (Color online) X-ray-induced scintillation decay curves of (a) 0.1PSAT glass, (b) 0.5PSAT glass, and (c) 1.0PSAT glass.

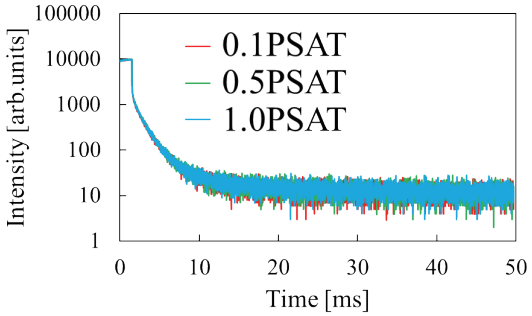

Fig. 11. (Color online) Afterglow profiles of the PSAT glasses.

complex processes at shallow traps should affect the afterglow levels. In this work, the afterglow level decreased with increasing amount of Pr_2O_3, suggesting that the number of shallow trapping centers is decreased by Pr_2O_3 doping. The decrease in the afterglow level upon Pr_2O_3 doping was found to be consistent with the discussion on the X-ray-induced scintillation spectra shown in Fig. 8.

4. Conclusion

$SrO–Al_2O_3–TeO_2$ glasses with different Pr_2O_3 concentrations (0.1, 0.5, 1.0%) were fabricated by the melt-quenching technique and their luminescence characteristics were investigated. Regarding their PL and scintillation properties, the PSAT glasses showed emissions originating from the 4f–4f transitions of Pr^{3+} with their typical decay times of the transitions in PL and scintillation. Furthermore, the afterglow levels of the PSAT glasses were calculated, and the 1.0PSAT glass showed a low afterglow level (352 ppm) comparable to that of the Tl-activated CsI single crystal. In this study, the 1.0PSAT glass was found to show the highest scintillation intensity and the lowest afterglow level. To improve the scintillation properties, it is necessary to optimize the glass composition and the species of the luminescence centers.

References

1 M. J. Weber: Nucl. Istrum. Methods Res. A. **527** (2004) 9.
2 E. Longo: Nucl. Instrum. Methods. Phys. Res., Sect. A **486** (2002) 7.
3 P. Lecoq: Nucl. Instrum. Methods. Phys. Res., Sect. A **809** (2016) 130.

4 N. Kawano, K. Shinozaki, M. Akatsuka, H. Kimura, D. Nakauchi, and T. Yanagida: Ceram. Int. **47** (2021) 11596.
5 Y. Isokawa, H. Kimura, T. Kato, N. Kawaguchi, and T. Yanagida: Opt. Mater. **90** (2019) 187.
6 H. Fukushima, M. Akatsuka, H. Kimura, D. Onoda, D. shiratori, D. Nakauchi, T. Kato, N. Kawaguchi, and T. Yanagida: Sens. Mater. **33** (2021) 2235.
7 K. Shinozaki, Y. Fujimoto, G. Okada, N. Kawaguchi, T. Yanagida, T. Akai, M. Koshimizu, and K. Asai: J. Mater. Sci. Mater. Electron. **29** (2018) 11824.
8 D. Shiratori, D. Nakauchi, H. Fukushima, T. Kato, N. Kawaguchi, and T. Yanagida: Opt. Mater. **105** (2020) 109895.
9 N. Kawaguchi, H. Masai, M. Akatsuka, D. Nakauchi, T. Kato, and T. Yanagida: Sens. Mater. **33** (2021) 2215.
10 H. Samizo, T. Kato, N. Kawaguchi, G. Okada, N. Kawaguchi, and T. Yanagida: J. Mater. Sci. Mater. Electron. **29** (2018) 1985.
11 N. Kawano, N. Kawaguchi, G. Okada. Y. Fujimoto, and T. Yanagida: Optik **224** (2020) 165613.
12 N. Kawano, K. Shinozaki, M. Akatsuka, H. Kimura, D. Nakauchi, and T. Yanagida: Ceram. Int. **47** (2021) 11596.
13 M. Seshadri, V. Anjos, and M. J. V. Bell: J. Lumin. **196** (2018) 399.
14 T. Hayakawa. M. Hayakawa, M. Nogami, and P. Thomas: Opt. Mater. **32** (2010) 448.
15 N. Kawano, H. Kimura, A. Horimoto, K. Shinozaki, and T. Yanagida: J. Mater. Sci. Mater. Electron. **30** (2019) 11468.
16 N. Kawano, H. Kimura, D. Nakauchi, K. Shinozaki, and T. Yanagida: Solid. Stat. Sci. **100** (2020) 106111.
17 A. Takaku, N. Kawano, H. Kimura, D. Nakauchi, M. Akatsuka, K. Shinozaki, and T. Yanagida: J. Ceram. Soc. Jpn. **128** (2020) 1024.
18 R. Nakamori, N. Kawano, A. Takaku, D. Kimura, M. Akatsuka, K. Shinozaki, and T. Yanagida: Mater. Res. Bull. **145** (2022) 111547.
19 V. H. Rao, P. S. Prasad, and K. S. Babu: Opt. Mater. **101** (2020) 109740.
20 H. Fukushima, D. Nakauchi, N. Kawaguchi, and T. Yanagida: J. Ceram. Process. Res. **20** (2019) 211.
21 N. Kumamoto, D. Nakauchi, T. Kato, G. Okada, N. Kawaguchi, and T. Yanagida: Optik **131** (2017) 957.
22 T. Yanagida, K. Kamada, Y. Fujimoto, H. Yagi, and T. Yanagitani: Opt. Mater. **35** (2013) 2480.
23 T. Yanagida, Y. Fujimoto, T. Ito, K. Uchiyama, and K. Mori: Appl. Phys. Express **7** (2014) 062401.
24 N. Kawano, K. Shinozaki, D. Nakauchi, H. Kimura, M. Akatsuka, and T. Yanagida: Radiat. Phys. Chem. **190** (2022) 109785.
25 R. N. A. Prasad, B. V. Siva, K. Neeraja, N. K. Mohan, and J. I. Rojas: J. Lumin. **230** (2021) 117666.
26 J. Hao, Z. Xu, R. Chu, W. Li, P. Fu, J. Du, and G. Li: J. Eur. Ceram. Soc. **37** (2017) 877.
27 D. Peng, H. Sun, X. Wang, J. Zhang, M. Tang, and X. Yao: J. Alloys Compd. **511** (2012) 159.
28 L. A. Deltreggia, M. I. B. Bernardi, and A Mesquita: Scr. Mater. **157** (2018) 15.
29 W. Dong, Y. Sun, Q. Yao, L. Liu, Q. Wang, H. Wen, J. Li, X. Xu, J. Wang, and R. I. Boughton: J. Lumin. **225** (2020) 117288.
30 D. Nakauchi, T. Kato, N. Kawaguchi, and T. Yanagida: Radiat. Phys. Chem. **182** (2021) 109390.
31 D. Nakauchi, G. Okada, M. Koshimizu, and T. Yanagida: Radiat. Meas. **106** (2017) 170.
32 D. J. Robbins: J. Electrochem. Soc. **127** (1980) 2694.
33 Y. Fujimoto, D. Nakauchi, T. Yanagida, M. Koshimizu, and K. Asai: Sens. Mater. **33** (2021) 2147.
34 M. Bliss, R. A. Craig, and P. L. Reeder: Nucl. Instrum. Methods. Phys. Res., Sect. A **342** (1994) 357.
35 A. G. Kalampounias: Bull. Mater. Sci. **31** (2008) 781.
36 N. Manikandan, A. Ryasnyanskiy, and J. Toulouse: J. Non-Cryst. Solids **358** (2012) 947.
37 K. Kagami, Y. Fujimoto, M. Koshimizu, D. Nakauchi, T. Yanagida, and K. Asai: Opt. Mater. **87** (2019) 127.
38 K. Igashira, D. Nakauchi, Y. Fujimoto, T. Kato, N. Kawaguchi, and T. Yanagida: Opt. Mater. **98** (2019) 109497.